Variance Analysis for Monte Carlo Integration
Supplementary material

†Adrien Pilleboue[1,⋆] †Gurprit Singh[1,⋆] David Coeurjolly[2,⋆] Michael Kazhdan[3,∗] Victor Ostromoukhov[1,2,⋆]
†*joint first authors* [1]Université Lyon 1 [2]CNRS/LIRIS UMR 5205 [3]Johns Hopkins University

1 Overview

In this document, we provide supplementary details on various topics discussed from the main paper. In Sec. 2, we give a short background of the *Representation theory* framework that we used in our derivation for the spherical domain Monte Carlo (MC) variance formulation. In Sec. 3, we provide additional theoretical background of *projective 2-space* that allows spectral analysis of hemispherical signals using spherical harmonics. In Sec. 4, we study the best- and worst-case integrands used for experiments in the main paper. We show that both the disk function and the spherical cap function follows the spectral decay rate as predicted by Brandolini and colleagues in [2001]. In Sec. 5, we provide extra experimental details on various test integrands used to sudy the convergence rate of various sampling patterns. We conclude this document by providing extra results.

2 Background on Representation theory

In the main paper *(Sections 4 and 5, MC variance analysis in* $\mathcal{T}^d/\mathcal{S}^2$*)* we present expressions for the variance of homogenuous sampling patterns in Euclidean space and on the (hemi-)sphere. For both, we obtain the expressions by considering the average of the product of Fourier/Harmonic coefficients over translations/rotations of the sampling pattern. Leveraging a *Representation Theory* framework, we derive closed-form expression for the average. In this section, we briefly review some aspects of the Representation theory used in the main paper:

Definition Given a complex inner-product space $(V, \langle\cdot,\cdot\rangle)$ and compact group H, we say that the map $\rho : H \to U(V)$ (with $U(V)$ the group of unitary transformations on V) is a *representation* if:

$$\rho(h_0 \cdot h) = \rho(h_0) \circ \rho(h), \qquad \forall h_0, h \in G. \tag{1}$$

Notation Given a representation $\rho : H \to U(V)$, $h \in H$, and $v \in V$, we will write:

$$h(v) \equiv \rho(h)(v). \tag{2}$$

Definition Given a representation $\rho : H \to U(V)$ and a subspace $W \subset V$, we say that W is a *sub-representation* if $h(w) \in W$ for all $w \in W$ and all $h \in H$.

Definition Given a representation $\rho : H \to U(V)$ we say that V is an *irreducible representation* if the only sub-representations are the trivial ones, $W = \{0\}$ and $W = V$.

Now, we give the closed-form expressions for the average:

Proposition 2.1. *Given an irreducible representation* $\rho : h \to U(V)$*, for any* $x, y, v, w \in V$*, we have:*

$$\int_H \langle x, h(y)\rangle \ \overline{\langle v, h(w)\rangle}\, \mathsf{d}h = \frac{\mu(H)}{dim(V)} \langle x, v\rangle \ \overline{\langle y, w\rangle}\,. \tag{3}$$

where $\langle\ ,\ \rangle$ *represents an inner product operator.*

⋆ firstname.lastname@liris.cnrs.fr
∗ misha@cs.jhu.edu

Proof Fixing $y, w \in V$, let $B_{y,w} : V \times V \to \mathbb{C}$ be the map:

$$B_{y,w}(x, v) = \int_{h\in H} \langle x, h(y)\rangle \ \overline{\langle v, h(w)\rangle}\, \mathsf{d}h. \tag{4}$$

It is not hard to show that this map is linear in the first argument, conjugate-linear in the second, and H-equivariant. (That is, for any $h_0 \in H$ we have $B_{v,w}\left(h_0(x), h_0(y)\right) = B_{v,w}(x, y)$). Thus, by Schur's Lemma [Serre 1977; Fulton and Harris 1991], $B_{y,w}$ is a scalar multiple of the inner-product on V:

$$B_{y,w}(x, v) = \lambda_{y,w} \langle x, v\rangle\ . \tag{5}$$

Noting that this satisfies $B_{y,w}(x, v) = \overline{B_{x,v}(y, w)}$, it follows that:

$$B_{y,w}(x, v) = \lambda\ \langle x, y\rangle\ \overline{\langle v, w\rangle}\,, \tag{6}$$

for some constant $\lambda \in \mathbb{C}$ that is independent of v and w. Finally, letting $\{v_1, \ldots, v_n\}$ be an orthonormal basis for V, we can express the integral of the square norm of the trace of $\rho(h)$ as:

$$\begin{aligned}\int_H \left\|\mathrm{Tr}\left(\rho(h)\right)\right\|^2 \ \mathsf{d}h &= \int_H \left\|\sum_{i=1}^{n} \langle h(v_i), v_i\rangle\right\|^2 \ \mathsf{d}h \\ &= \sum_{i,j=1}^{n} B_{v_j,v_i}(v_j, v_i) \\ &= \dim(V) \cdot \lambda.\end{aligned}$$

Since the trace is the character of the representation, it follows by the orthogonality of characters [Serre 1977; Fulton and Harris 1991] that $\int_H \left\|\mathrm{Tr}\left(\rho(h)\right)\right\|^2 \ \mathsf{d}h = \mu(H)$, which gives:

$$\lambda = \frac{\mu(H)}{\dim(V)}. \tag{7}$$

Thus, we get:

$$\int_H \langle x, h(y)\rangle \ \overline{\langle v, h(w)\rangle}\, \mathsf{d}h = \frac{\mu(H)}{\dim(V)} \langle x, v\rangle \ \overline{\langle y, w\rangle}\,. \tag{8}$$

□

Proposition 2.2. *Leveraging Schur's Lemma in a similar manner, it follows that if* $\rho_1 : h \to U(V_1)$ *and* $\rho_2 : h \to U(V_2)$ *are two irreducible representations that are not isomoprhic, then for any* $v_1, w_1 \in V_1$ *and* $v_2, w_2 \in V_2$*:*

$$\int_H \langle v_1, h(w_1)\rangle \ \overline{\langle v_2, h(w_2)\rangle}\, \mathsf{d}h = 0. \tag{9}$$

We use Propositions 2.1 and 2.2 in *Section 5.2* of the main paper to derive the variance closed-form expression in the spherical domain.

Euclidean domain The variance equation derived in *Section 4.2* of the main paper for the Euclidean case, can also seen as a realization of Propositions 2.1 and 2.2. From *Eq. (E-10), of the main*

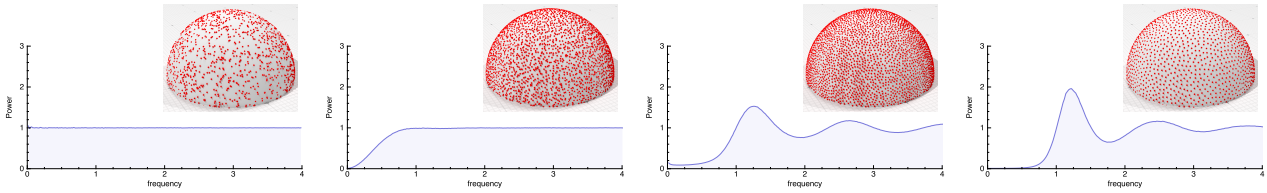

(a) Whitenoise (b) Jittered (c) Poisson disk (d) CCVT

Figure 1: *Comparison of the power spectra of various state of the art sampling patterns in the hemispherical domain. To perform spectral analysis, we used spherical harmonics after mapping the hemispherical sampling pattern to the projective 2-space, as discussed in Sec. 3.*

paper, we can observe that the ω-th Fourier coefficient of F can be expressed as the dot-product:

$$\mathcal{F}_F(\omega) = F(x) \cdot e^{i2\pi x \cdot \omega} = \int_{\mathcal{T}^d} F(x)\overline{e^{i2\pi x \cdot \omega}} \mathrm{d}x \,. \qquad \text{(E–10)}$$

Here, we consider the irreducible representations $V^\omega = Span\{e^{2\pi i \omega \cdot x}\}$ under the action of the group of translations. In this context, Proposition 2.2 implies that we can ignore cross-frequency terms, replacing the double integral over $\Theta \times \Theta$ with the single integral over Θ, and Proposition 2.1 gives the average square-norm of the ω-th Fourier coefficient of the sampling pattern, taken over all translational shifts.

3 MC variance analysis on Hemisphere

As discussed in the paper (*Section 5.2, Variance in spectral form in spherical domain*), we can apply the mathematical procedure developed on the sphere, in the hemispherical domain, to perform MC variance analysis on the hemisphere using spherical harmonics. This is possible due to the fact that the sphere is a Riemannian double-cover of *projective 2-space* and all local geometric calculations in the spherical domain are applicable on hemispherical functions if we associate the hemisphere to the *projective 2-space*. Here we use the fact that, any function on *projective 2-space* can be extended to an even function on the sphere.

Projective 2-space ($\mathbb{P}^2$) is defined to be the set of points on the sphere, modded out by the relation that for all $x \in \mathbb{P}^2$, x and $-x$ belongs to the same equivalence class. Then given a function on the projective 2-space, $\mathrm{G} \in L^2(\mathbb{P}^2)$, it can be turned into a function on the sphere by setting the value at the points x and $-x$ to be the value of G on the equivalence class $\{x, -x\}$. In particular, this means that the space of functions on *projective 2-space* is the same as the space of *even* functions on the sphere. Thus, rotation can be defined on $L^2(\mathbb{P}^2)$ by treating the function as an even function on the sphere, rotating the even function (which remains even after rotation) and then considering the corresponding function on *projective 2-space*. In that case, all the results derived in the spherical domain follow, including the *homogeneous property*. The space of even functions on the sphere is precisely the space of functions spanned by spherical harmonic basis functions of even degree, Y_m^l with l even. The only assumption here is that we restrict our analysis to functions on the hemisphere with $\mathrm{G}(x) = \mathrm{G}(-x)$ for all points on the equator.

Spectral analysis of sampling patterns We perform spectral analysis on the hemispherical sampling patterns (in Fig. 1) by first associating the hemispherical samples to the projective 2-space and then computing angular power spectra using spherical harmonics.

4 Best and worst case study

In the main paper *(Section 6)*, we discuss our best- and worst-case of integrands for the Euclidean and the spherical domains by considering the fact that the power spectrum of an integrand defined in $\mathcal{T}^d$ is bounded. In this section (Sec. 4.1) we give a formal proof of this statement. Later, in Sec. 4.2 and 4.3, we study our worst-case function used in the Euclidean and spherical domains. We first study the characteristic disk function, and prove that the power spectrum ($\tilde{\mathcal{P}_F}(\cdot)$) decay rate of the d-dimensional disk function is the same as the one advocated by Brandolini and colleagues [2001] and later focus on the spherical cap function.

4.1 Bound of the Power Spectrum

Lemma 4.1. *The power spectrum $\mathcal{P}_g$ of the d-dimensional function g is bounded by the square of the L^1 norm of g.*

Proof From Fourier transform of g:

$$\mathcal{F}_g(\omega) = \int_{\mathbb{R}^d} g(\mathbf{x}) e^{-i2\pi\omega\mathbf{x}} \mathbf{dx} \,, \qquad \text{(E–11)}$$

the amplitude of the Fourier transform of g can be bounded by the L^1 norm of g:

$$\begin{aligned} |\mathcal{F}_g(\omega)| &= \left| \int_{\mathbb{R}^d} g(\mathbf{x}) e^{-i2\pi\omega\mathbf{x}} \mathbf{dx} \right| \\ &\leqslant \int_{\mathbb{R}^d} |g(\mathbf{x})||e^{-i2\pi\omega\mathbf{x}}| \mathbf{dx} \\ &\leqslant \int_{\mathbb{R}^d} |g(\mathbf{x})| \mathbf{dx} \,. \end{aligned} \qquad \text{(E–12)}$$

Since $\mathcal{P}_g(\omega) = |\mathcal{F}_g(\omega)|^2$, the power spectrum of g is bounded by the square of the L^1 norm of g. □

4.2 Assymptotic Behaviour of d-dimensional disk Power spectrum

Lemma 4.2. *The radial power spectrum $\mathcal{P}_d$ of a d-dimensional disk is in $O(\omega^{-(d+1)})$.*

Proof First of all, the radial Fourier transform $\mathcal{F}_d(\rho)$ of a d-dimensional disk is given by:

$$\mathcal{F}_d(\rho) = 2^{d/2}\Gamma(d/2+1)\frac{J_{d/2}(2\pi\rho)}{(2\pi\rho)^{d/2-1}} \,, \qquad \text{(E–13)}$$

with $J_\nu(\rho)$ being the order-ν Bessel function [Vembu 1961]. For $\nu \geq 0$, $|J_\nu(\rho)|$ is in $O(\rho^{-1/2})$ [Olenko 2006]. As a consequence, $|\mathcal{F}_d(\rho)|$ is in $O(\rho^{-(d+1)/2})$ leading to $\mathcal{P}_d(\rho) = O(\rho^{-(d+1)})$. □

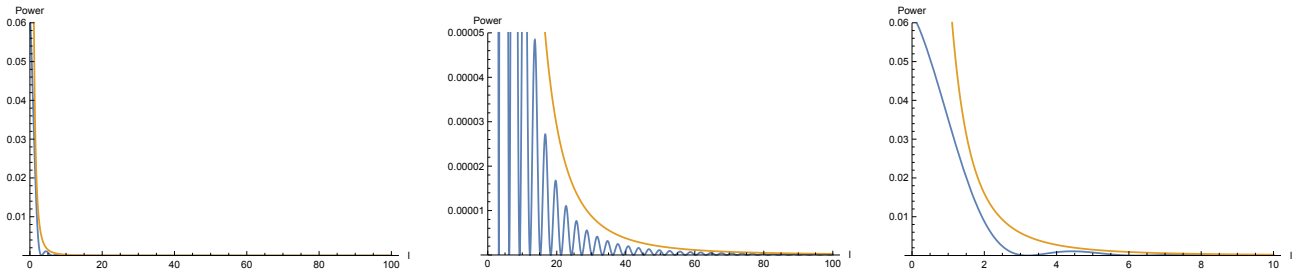

(a) (b) (c)

Figure 2: *We illustrate the power profile (Power vs l) of a spherical cap function (in blue) for $\theta_0 = 60$ with the corresponding bound (in orange). We show three plots of the same power spectrum (a), with different zoom-in plots, (b) and (c), to better see the upper bound and to show that the power of the spherical cap is well bounded by the upper bound we derived in Sec. 4.4.*

4.3 Spherical cap function in SH terms

In the main paper *(Section 6 and 8)*, we consider a spherical cap function as our worst-case integrand for a given class of functions. We compute an analytical expression for the power spectrum of a spherical cap function. For simplicity sake, we define spherical cap function, $F_{\theta_0}(\theta)$, as a circularly symmetric spherical cap centered at the north pole as a function of the colatitude $\theta \in [0, \pi]$:

$$F_{\theta_0}(\theta) = \begin{cases} 1 & \text{if } \theta \leq \theta_0 \\ 0 & \text{otherwise} \end{cases}, \tag{S–14}$$

where, $\epsilon < \theta_0 < \pi - \epsilon$, is a constant that controls the size of the spherical cap, for $\epsilon > 0$. Since F_{θ_0} is circularly symmetric, we can consider only the zonal ($m = 0$) harmonic basis functions. Hereafter, we drop the subscript θ_0 from F_{θ_0} to denote spherical cap function and express it as F. To obtain spectral coefficients ($\mathcal{S}_F(l, 0)$) of the spherical cap function, we simply take its inner product—denoted by $\langle \cdot, \cdot \rangle$—with the zonal components of the spherical harmonics:

$$\begin{aligned}
\mathcal{S}_F(l,0) &= \langle F_{\theta_0}(\theta), Y_l(\theta,\phi)\rangle && \text{(S–15)}\\
&= \int_{\theta=0}^{\pi}\int_{\phi=0}^{2\pi} \mathrm{F}_{\theta_0}(\theta)\, Y_l(\theta,\phi)\sin\theta d\phi d\theta && \text{(S–16)}\\
&= \int_{\theta=0}^{\theta_0}\int_{\phi=0}^{2\pi} Y_l(\theta,\phi)\sin\theta d\phi d\theta && \text{(S–17)}\\
&= \sqrt{2l+1}\int_{\theta=0}^{\theta_0}\int_{\phi=0}^{2\pi} P_l^0(\theta,\phi)\sin\theta d\phi d\theta && \text{(S–18)}\\
&= \sqrt{2l+1}\int_{\theta=0}^{\theta_0}\int_{\phi=0}^{2\pi} P_l^0(\cos\theta)\sin\theta d\phi d\theta && \text{(S–19)}\\
&= \sqrt{2l+1}\int_{\theta=0}^{\theta_0}\left(\int_{\phi=0}^{2\pi} d\phi\right) P_l^0(\cos\theta)\sin\theta d\theta && \text{(S–20)}\\
&= \sqrt{2l+1}\int_{\theta=0}^{\theta_0} 2\pi P_l^0(\cos\theta)\sin\theta d\theta && \text{(S–21)}\\
&= 2\pi\sqrt{2l+1}\int_{\theta=0}^{\theta_0} P_l^0(\cos\theta)\sin\theta d\theta\,. && \text{(S–22)}
\end{aligned}$$

Legendre polynomials satisfy:

$$(2l+1)P_l^0(x) = \frac{d}{dx}\left[P_{l+1}^0(x) - P_{l-1}^0(x)\right]. \tag{S–23}$$

Substituting Eq. (S–23) in Eq. (S–22), we get:

$$\mathcal{S}_F(l,0) = 2\pi\left(\frac{P_{l-1}^0(\cos(\theta_0) - P_{l+1}^0(\cos\theta_0)}{\sqrt{2l+1}}\right), \tag{S–24}$$

which is the expression for the spherical cap harmonic coefficients $\mathcal{S}_F(l, 0)$ in terms of l and θ_0. As shown in the paper, the variance in numerical integration for MC integration is directly related to the $||\mathcal{S}_F(l,0)||^2$ of the integrand. Here, our integrand is a spherical cap function and the corresponding $||\mathcal{S}_F(l,0)||^2$ is given by:

$$||\mathcal{S}_F(l,0)||^2 = 4\pi^2\left(\frac{|P_{l-1}^0(\cos(\theta_0) - P_{l+1}^0(\cos\theta_0)|^2}{2l+1}\right), \tag{S–25}$$

We use Eq. (S–25) in the *angular* power spectrum definition (*given in the main paper, Section 5.2*) to numerically compute the bounds on the associated variance of the spherical cap for various state-of-the-art sampling patterns, as shown *in Fig. 6 of the main paper*. We would like to set an upper bound on $||\mathcal{S}_F(l,0)||^2$ given in Eq. (S–25). This expression contains the shifted copies (with respect to l) of the associated Legendre Polynomial $P_l(x) := P_l^0(x)$. We can first upper bound the term $|P_{l-1}(\cos\theta_0) - P_{l+1}(\cos\theta_0)|$. Several sharp estimations can be found in the literature for the Legendre polynomial $P_l(x)$. A classical result for $x \in]-1, 1[$ and $l \in \mathbb{N}$, is the improved version of *Bernstein's inequality*, [Lohöfer 1998; Lorch 1983], given by:

$$|P_l(x)| < \sqrt{\frac{2}{\pi(l+1/2))}}\frac{1}{(1-x^2)^{\frac{1}{4}}}. \tag{S–26}$$

For $x = \cos\theta_0$, this inequality becomes:

$$|P_l(\cos\theta_0)| < \sqrt{\frac{2}{\pi(l+1/2))}}\frac{1}{\sqrt{\sin\theta_0}} = \frac{2}{\sqrt{(2l+1)\pi\sin\theta_0}}. \tag{S–27}$$

We treat $l = 0$ as a special case. For $l > 0$, using the above inequality in Eq. (S–27) we can derive:

$$|P_{l-1}(\cos\theta_0)| < \frac{2}{\sqrt{(2l-1)\pi\sin\theta_0}}, \tag{S–28}$$

and,

$$|P_{l+1}(\cos\theta_0)| < \frac{2}{\sqrt{(2l+3)\pi\sin\theta_0}} < \frac{2}{\sqrt{(2l-1)\pi\sin\theta_0}}, \tag{S–29}$$

without any loss of generality. From triangular inequality, we get:

$$|P_{l-1}(\cos\theta_0) - P_{l+1}(\cos\theta_0)| < |P_{l-1}(\cos\theta_0)| + |P_{l+1}(\cos\theta_0)|. \tag{S–30}$$

Using Eq. (S–28) and Eq. (S–29) in the above expression, gives us:

$$|P_{l-1}(\cos\theta_0) - P_{l+1}(\cos\theta_0)| < \frac{4}{\sqrt{(2l-1)\pi\sin\theta_0}}. \tag{S–31}$$

For $l > 0$, both left and right hand side of Eq. (S–31) are positive. Therefore, squaring followed by a division with $2l + 1 \geq 1$ on both sides, would not affect the inequality:

$$\frac{|P_{l-1}(\cos\theta_0) - P_{l+1}(\cos\theta_0)|^2}{2l+1} < \frac{16}{(2l+1)(2l-1)\pi\sin\theta_0}\,. \tag{S–32}$$

Plugging this in Eq. (S–25), gives us the upper bound on the power spectrum of the spherical cap function for any θ_0 and $l > 0$, which can be written as:

$$\boxed{||\mathcal{S}_F(l,0)||^2 < \frac{64\pi}{\sin\theta_0}\left(\frac{1}{(2l+1)(2l-1)}\right)}\,. \tag{S–33}$$

For $l = 0$: Associated Legendre polynomials have a property according to which $P_{-1}(x) = P_0(x)$, that gives:

$$|P_{l-1}(\cos\theta_0)| = |P_{-1}(\cos\theta_0)| = |P_0(\cos\theta_0)| < \frac{2}{\sqrt{\pi\sin\theta_0}}\,, \tag{S–34}$$

$$|P_{l+1}(\cos\theta_0)| = |P_1(\cos\theta_0)| < \frac{2}{\sqrt{3\pi\sin\theta_0}} < \frac{2}{\sqrt{\pi\sin\theta_0}}\,, \tag{S–35}$$

$$|P_0(\cos\theta_0) - P_1(\cos\theta_0)| < \frac{4}{\sqrt{\pi\sin\theta_0}}\,, \tag{S–36}$$

$$|P_0(\cos\theta_0) - P_1(\cos\theta_0)|^2 < \frac{16}{\pi\sin\theta_0}\,, \tag{S–37}$$

using the above inequality in Eq. (S–25), for $l = 0$, gives us the upper bound on:

$$\boxed{||\mathcal{S}_F(0,0)||^2 < \frac{64\pi}{\sin\theta_0}}\,. \tag{S–38}$$

The inequality in Eq. (S–33) does not gaurantee a (very) tight bound on the power of the spherical cap coefficients. However, for our analysis we found that this bound can still be used to conjecture the rate of convergence for the worst-case error in integration.

4.4 Spherical cap power spectrum

To study the worst-case, we are looking for a function with squared-norm zonal spectral coefficients, $||\mathcal{S}_F(l,0)||^2$, exhibiting a decay rate of order $O(l^{-2})$, as derived by Brandolini in [2001]. We have shown in the previous subsection 4.3, that a spherical cap function has this behaviour (Eq. (S–33)). The corresponding *angular* power spectrum decay rate can be obtained using Eq. (S–33) in the definition of the *angular power spectrum*. The resulting decary rate of the angular power spectrum for a spherical cap is given by:

$$\boxed{\breve{\mathcal{P}}_F(l) < \frac{C_0}{(2l+1)^2(2l-1)}}\,, \tag{S–39}$$

where $C_0 = 64\pi/(\sin\theta_0)$. In Fig. 2, we show an illustration of this upper bound on a spherical cap function of size $\theta_0 = 60$. We can derive a correspoding worst-case variance convergence rate using Eq. (S–39) given by:

$$Var\left(\boldsymbol{I}_N\right) < \frac{\mu(\mathcal{S}^2)^2\, C_0}{N} \sum_{l=0}^{\infty} \frac{\left\langle \breve{\mathcal{P}}_{\mathbf{S}}(l) \right\rangle}{(2l+1)(2l-1)}\,. \tag{S–40}$$

This variance bound can be used to study different shapes of the sampling power spectra ($\breve{\mathcal{P}}_{\mathbf{S}}(l)$) to derive their convergence rate with respect to the number of samples N.

5 Experimentation details

In the *Experiments and Results (Section 8)* of the main paper, we study the worst-case variance in integration for the given class of functions in the Euclidean and the spherical domain. We later study the behaviour of a Gaussian function and a spherical harmonic basis function. Below we provide details for each of the integrands:

Gaussian in $\mathcal{T}^2$ We consider a Gaussian function defined by:

$$F(x,y) = 8e^{-32\pi(x^2+y^2)}\,,$$

with the corresponding spectral profile given by:

$$\breve{\mathcal{P}}_F(\rho) = \frac{1}{16} e^{\frac{-\pi(\rho^2)}{16}}\,.$$

This integrand is not bandwidth-limited but smooth enough to have an exponential decay rate for its corresponding power spectral profile.

Disk in $\mathcal{T}^2$ For our worst-case in the given class of functions, we consider a circular disk in the Euclidean space, which has a spectral profile decay rate of the order proposed by Brandolini et al. [2001]. The disk is defined by:

$$F(x,y) = \begin{cases} 4/\sqrt{\pi}, & \text{if } \sqrt{x^2+y^2} < 1/4 \\ 0, & \text{otherwise.} \end{cases}$$

To fit the domain of integration, the disk is translated to the center of the domain of integration $(1/2, 1/2)$. Its spectral profile is given by:

$$\breve{\mathcal{P}}_F(\rho) = \frac{J_1(\pi\sqrt{\rho^2}/2)^2}{\pi(\rho^2)}\,,$$

where J_1 is a 1st order Bessel function.

Spherical harmonic basis function (Y_l^m) in $\mathcal{S}^2$ In the spherical domain, we chose a SH basis function Y_l^m with $(l = 4, m = 0)$, which is a band limited function. Y_0^4 is a smooth function with compact support and can be considered as a *best-case* for the class of functions discussed in the paper. The power spectral profile of any SH basis function, Y_m^l, is given by $\breve{\mathcal{P}}_F(l) = \mu(\mathcal{S}^2)/(2l+1)$, as $||Y_l^m||^2 = \mu(\mathcal{S}^2)$.

HDR image In *(Figure 4)*, we present integration results of HDR image. We want this case of integration as an illustration of a difficult but realistic case of integration. To ensure that the image is not too simple to integrate, we use a box filter, leading to high frequency content in the reconstructed image.

Extra results At the end of this document, we include some results, namely, rendering Cornell box scene with ambient occlusion, with reference image shown at the end of the document with the HDR image used to study the sampling pattern convergence behaviour for the Euclidean case.

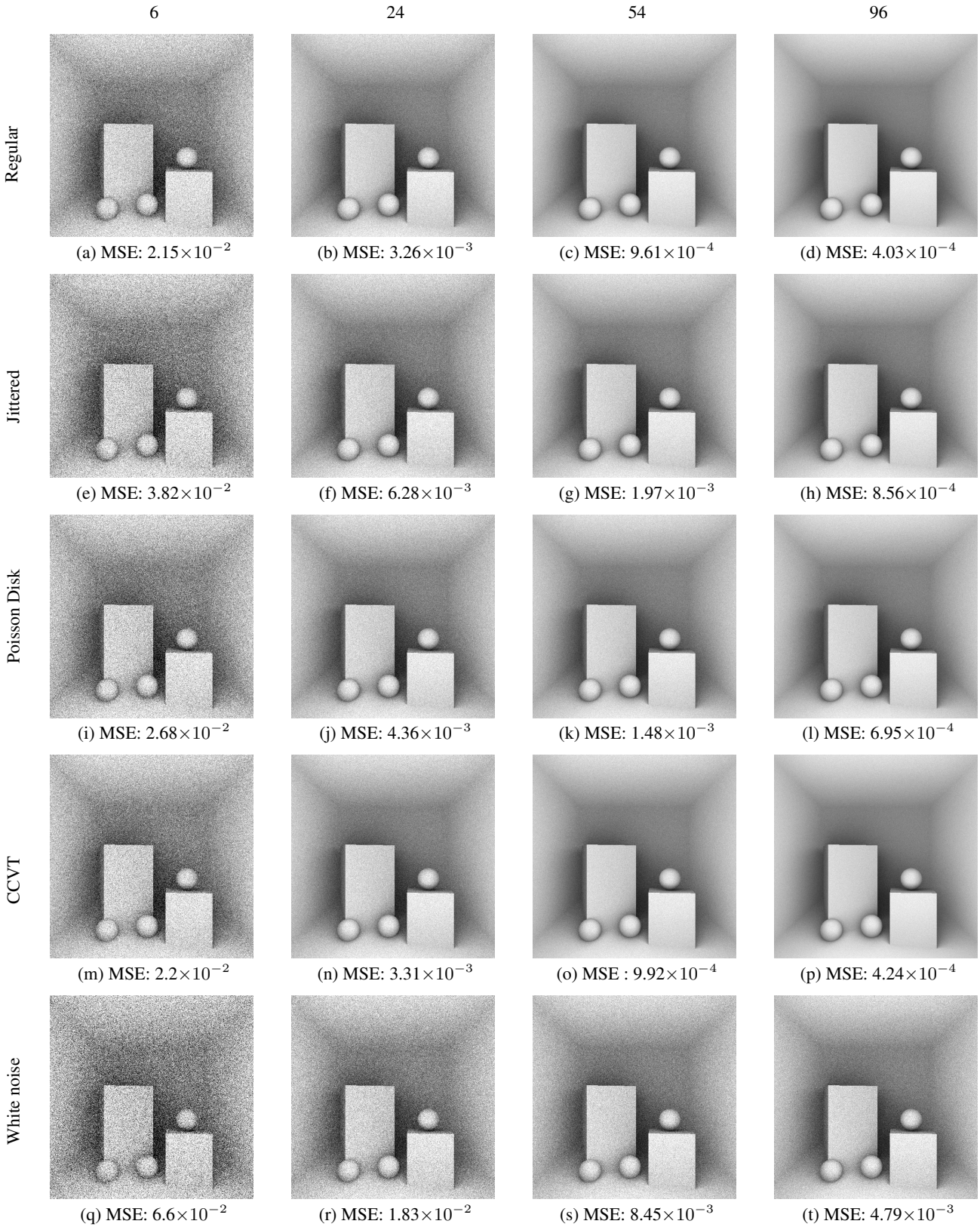

(a) MSE: 2.15×10^{-2} (b) MSE: 3.26×10^{-3} (c) MSE: 9.61×10^{-4} (d) MSE: 4.03×10^{-4}

(e) MSE: 3.82×10^{-2} (f) MSE: 6.28×10^{-3} (g) MSE: 1.97×10^{-3} (h) MSE: 8.56×10^{-4}

(i) MSE: 2.68×10^{-2} (j) MSE: 4.36×10^{-3} (k) MSE: 1.48×10^{-3} (l) MSE: 6.95×10^{-4}

(m) MSE: 2.2×10^{-2} (n) MSE: 3.31×10^{-3} (o) MSE : 9.92×10^{-4} (p) MSE: 4.24×10^{-4}

(q) MSE: 6.6×10^{-2} (r) MSE: 1.83×10^{-2} (s) MSE: 8.45×10^{-3} (t) MSE: 4.79×10^{-3}

Figure 3: *Cornell box rendered with ambient occlusion.* Mean squared error *(MSE) values are computed w.r.t a reference image (shown on the next page, Fig. 4) for each sampling pattern (mentioned in the left most column) for a given number of shading rays (top most row) used to sample directions on the visible hemisphere at each hitpoint in the scene.*

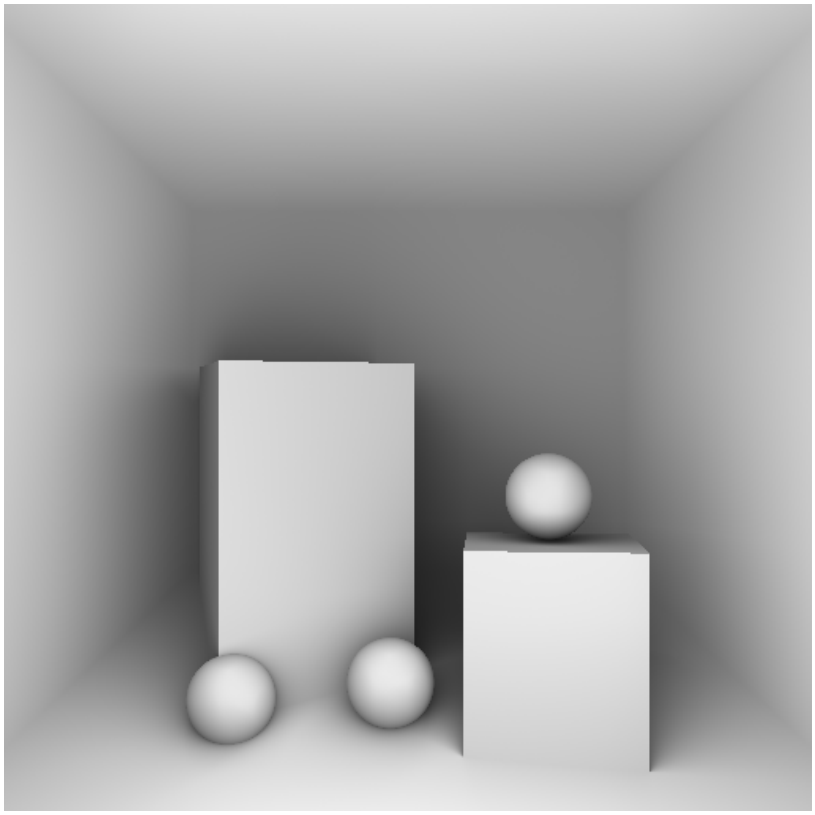

Figure 4: ***Top:*** *Original HDR image used in the paper, courtesy sIBL archive.* ***Bottom:*** *Cornell box reference image synthesized using* $32k$ *hemispherical jittered samples generated via Healpix data structure. In the paper we show this image as an inset in the comparison graphs.*

References

BRANDOLINI, L., COLZANI, L., AND TORLASCHI, A. 2001. Mean square decay of Fourier transforms in euclidean and non euclidean spaces. *Tohoku Math. J. (2) 53*, 3, 467–478.

FULTON, W., AND HARRIS, J. 1991. *Representation Theory: A First Course*. Springer-Verlag, New York.

LOHÖFER, G. 1998. Inequalities for the associated Legendre functions. *J. Approx. Theory 95*, 2, 178–193.

LORCH, L. 1983. Alternative proof of a sharpened form of Bernstein's' inequality for Legendre polynomials. *Applicable Analysis 14*, 3, 237–240.

OLENKO, A. Y. 2006. Upper bound on x j ν (x) and its applications. *Integral Transforms and Special Functions 17*, 6, 455–467.

SERRE, J. 1977. *Linear representations of finite groups*. Springer-Verlag, New York.

VEMBU, S. 1961. Fourier transformation of the n-dimensional radial delta function. *The Quarterly Journal of Mathematics 12*, 1, 165–168.